

# Real-Time Surface Plasmon Resonance Imaging Measurements for the Multiplexed Determination of Protein Adsorption/Desorption Kinetics and Surface Enzymatic Reactions on Peptide Microarrays

Greta J. Wegner, Alastair W. Wark,<sup>†</sup> Hye Jin Lee,<sup>†</sup> Eric Codner, Tomonori Saeki,<sup>‡</sup> Shiping Fang,<sup>†</sup> and Robert M. Corn<sup>\*,†</sup>

Department of Chemistry, University of Wisconsin, 1101 University Avenue, Madison, Wisconsin 53706

**The kinetics of protein adsorption/desorption onto peptide microarrays was studied using real-time surface plasmon resonance (SPR) imaging. S protein binding interactions were examined using an array composed of five different peptides: N terminal and C terminal immobilized wild-type S peptide (S1 and S2), an alternate binding sequence derived by phage display (LB2), an NVOC-protected S peptide, and a FLAG peptide control sequence (F). Kinetic measurements of the S protein–S1 peptide interaction were analyzed to determine a desorption rate constant ( $k_d$ ) of  $1.1 (\pm 0.08) \times 10^{-2} \text{ s}^{-1}$ , an adsorption rate constant ( $k_a$ ) of  $1.9 (\pm 0.05) \times 10^5 \text{ M}^{-1} \text{ s}^{-1}$ , and an equilibrium adsorption constant ( $K_{\text{Ads}}$ ) of  $1.7 (\pm 0.08) \times 10^7 \text{ M}^{-1}$ . SPR imaging equilibrium measurements of S protein to S1 peptide were performed to independently confirm the kinetically determined value of  $K_{\text{Ads}}$ . Rate constants for the S2 and LB2 peptides on the array were measured as follows:  $1.6 (\pm 0.04) \times 10^5 \text{ M}^{-1} \text{ s}^{-1}$  ( $k_a$ ) and  $1.1 (\pm 0.07) \times 10^{-2} \text{ s}^{-1}$  ( $k_d$ ) for S2,  $1.2 (\pm 0.05) \times 10^5 \text{ M}^{-1} \text{ s}^{-1}$  ( $k_a$ ) and  $1.1 (\pm 0.03) \times 10^{-2} \text{ s}^{-1}$  ( $k_d$ ) for LB2. In addition to S protein adsorption/desorption, real-time SPR imaging of peptide arrays was applied to study the surface enzymatic activities of the protease factor Xa. Enzymatic cleavage of the substrate peptide (P1) was shown to follow first-order kinetics and proceed at a rate 10 times faster than that of the mutant peptide (P2), with cleavage velocities of  $5.6 (\pm 0.3) \times 10^{-4} \text{ s}^{-1}$  for P1 and  $5.7 (\pm 0.3) \times 10^{-5} \text{ s}^{-1}$  for P2.**

Peptide–protein interactions are frequently studied in proteomics efforts to investigate molecular recognition and to develop therapeutic agents that alter these interactions. Protein–protein recognition often occurs through conserved sequence-specific regions on a protein. In many cases, the contribution of individual amino acids to a binding interaction or to an enzymatic activity

can be determined using sets of short peptide sequences.<sup>1–3</sup> Equilibrium affinity measurements of peptides and proteins can be used to study the sequence specificity of these interactions.

In addition to equilibrium measurements, kinetic measurements can provide further information about the mechanisms of protein–peptide binding and enzymatic reactions. For example, the kinetics of protein–peptide binding can provide insight about the conformation of the peptide ligand and the nature of the binding pocket.<sup>4–6</sup> Competitive adsorption/desorption measurements of inhibitors and native peptide ligands to relevant protein binding sites can be used to accelerate the selection of promising drug candidates. This tactic has been applied to a class of HIV drugs that prevent viral spread by blocking a protein–protein interaction necessary for protease activity.<sup>7–9</sup> In support of these studies, the effect of optimized inhibitors on the activity of enzyme variants can be compared to understand the evolution of drug resistance. These kinetic measurements are important to identify drug candidates that are effective against the structural variations of HIV protease present in different viral strains.<sup>10, 11</sup>

Peptide arrays are emerging as an effective tool to obtain multiplexed kinetics information for applications such as the development of HIV protease inhibitors. Extensive studies have

- (1) Pelloso, J. P.; Zhou, X.; Srivannavit, O.; Zhou, T.; Gulari, E.; Gao, X. *Nat. Biotechnol.* **2002**, *20*, 922–926.
- (2) Wenschuh, H.; Volkmer-Engert, R.; Schmidt, M.; Schulz, M.; Schneider-Mergener, J.; Reineke, U. *Biopolymers* **2000**, *55*, 188–206.
- (3) Reineke, U.; Volkmer-Engert, R.; Schneider-Mergener, J. *Curr. Opin. Biotechnol.* **2001**, *12*, 56–64.
- (4) Betts, R.; Weinsheimer, S.; Blouse, G. E.; Anagli, J. *J. Biol. Chem.* **2003**, *278*, 7800–7809.
- (5) Yang, J.; Swaminathan, C. P.; Huang, Y.; Guan, R.; Cho, S.; Kieke, M. C.; Kranz, D. M.; Mariuzza, R. A.; Sundberg, E. J. *J. Biol. Chem.* **2003**, *278*, 50412–50421.
- (6) Ishino, T.; Pasut, G.; Scibek, J.; Chaiken, I. *J. Biol. Chem.* **2004**, *279*, 9547–9556.
- (7) Tomasselli, A. G.; Heinrikson, R. L. *Biochim. Biophys. Acta* **2000**, *1477*, 189–214.
- (8) Markgren, P. O.; Schaal, W.; Hamalainen, M.; Karlen, A.; Hallberg, A.; Samuelsson, B.; Danielson, U. H. *J. Med. Chem.* **2002**, *45*, 5430–5439.
- (9) Archakov, A. I.; Govorun, V. M.; Dubanov, A. V.; Ivanov, Y. D.; Veselovsky, A.; Lewi, P.; Janssen, P. *Proteomics* **2003**, *3*, 380–391.
- (10) Ogden, R. *Infect. Dis. Ther.* **2003**, *30*, 523–553.
- (11) Klabe, R.; Bachelier, L. T.; Ala, P. J.; Erickson-Viitanen, S.; Meek, J. S. *Biochemistry* **1998**, *37*, 8735–8742.

\* To whom correspondence should be addressed. E-mail: rcorn@uci.edu.

<sup>†</sup> Current address: Department of Chemistry, University of California, Irvine, CA 92697-2025.

<sup>‡</sup> Current address: Hitachi Production Engineering Research Laboratory, Yokohama, 244-0817 Japan.

previously demonstrated the utility of peptide arrays to characterize the sequences involved in protein–protein interactions,<sup>12–15</sup> to understand enzymatic activity,<sup>16–19</sup> and to develop artificial substrates to assist in drug design and clinical assays.<sup>20–23</sup> We have recently applied peptide arrays to the study of equilibrium bioaffinity antibody interactions with peptide epitopes using label-free surface plasmon resonance (SPR) imaging for detection.<sup>24</sup> SPR avoids the inconvenience and potential alteration of biological activity associated with the use of fluorescent tags. Another strength of SPR is the utility of angle-shift measurements (Biacore, HTS Biosystems, Texas Instruments) for kinetics studies of biomolecular interactions.<sup>25–27</sup> Recently, time-resolved SPR measurements in an imaging format have been reported by Campbell et al. for the study of a streptavidin/biotin system.<sup>28,29</sup> All of these studies indicate that SPR imaging should be extremely useful for multiplexed kinetic measurements of protein interactions using peptide arrays.

In this paper, we demonstrate the use of real-time SPR imaging of peptide arrays to rapidly obtain multiplexed kinetic information about protein–peptide adsorption and surface enzyme reactions. To support this endeavor, a poly(dimethylsiloxane) (PDMS) microfluidic handling system was designed to facilitate well-controlled and reproducible analyte delivery to each element on the array surface. Two protein–peptide systems were studied: (1) the adsorption and desorption of S protein to S peptide derivatives, a binding pair frequently used in the purification of fusion proteins, and (2) the sequence-specific proteolytic cleavage of peptides by the protease factor Xa, which plays an important role in thrombosis and in clinical assays. The adsorption rate constants ( $k_a$ ), desorption rate constants ( $k_d$ ), and equilibrium adsorption constants ( $K_{Ads}$ ) for multiple S peptide derivatives were first determined by monitoring S protein binding to multicomponent peptide arrays using real-time SPR imaging. The sequence-specific activity of the

Table 1. Peptide Sequences for S Protein and Factor Xa Imaging Experiments

peptide	sequence (N to C terminus)	associated protein
S1	CSGKETAAAKFERQHMSD	S protein
S2	KETAAAKFERQHMDSSGC	S protein
LB2	CSGSGKETAWAIFVRQHMSD	S protein
P1	CSGIEGRDYKDDDDK	factor Xa
P2	CSGIEGADYKDDDDK	factor Xa
F	CSGDYKDDDDK	anti-FLAG

protease factor Xa was also studied by determining the difference in cleavage rates between a peptide substrate and a mutant peptide substrate, differing by a single amino acid.

## EXPERIMENTAL SECTION

**Materials.** *N*-Succinimidyl 3-(2-pyridylthio)propionamide (SPDP, Pierce), 11-mercaptoundecylamine (MUAM, Dojindo Laboratories), *N*-hydroxysuccinimidyl ester of methoxypoly(ethylene glycol) propionic acid MW 2000 (PEG-NHS, Nektar Therapeutics), S protein (Novagen), factor Xa (Amersham Biosciences), and 6-nitroveratryloxycarbonyl chloride (NVOC-Cl, Aldrich) were used as received without further purification. All rinsing steps were performed with Millipore filtered water and absolute ethanol. Phosphate buffer (10 mM Na<sub>2</sub>HPO<sub>4</sub>, 2.7 mM KCl, 137 mM NaCl) was used for all S protein adsorption and desorption experiments, while Tris buffer (50 mM Tris-HCl, 100 mM NaCl, 5 mM CaCl<sub>2</sub>, pH 8.0) was used for factor Xa reactions. Peptides were synthesized at the University of Wisconsin Biotechnology Center or Washington Biotechnology. Purity was determined using MALDI-TOF mass spectrometry and HPLC. The peptide sequences are listed in Table 1.

**Peptide Array Fabrication.** A multistep fabrication process was employed in the creation of robust peptide arrays for SPR imaging measurements. Substrates were prepared using a Denton DV-502A evaporator to vapor deposit thin gold films (45 nm) with an underlayer of chromium (1 nm) onto SF10 glass slides (Schott Glass). The gold substrate was then modified with an amine-terminated self-assembled monolayer (MUAM). Next, parallel microchannels (300- $\mu$ m width, 14.2-mm length, 35- $\mu$ m depth) with 700- $\mu$ m spacing between channels were placed on the gold substrate. Microchannels were fabricated by curing PDMS polymer on 3-D silicon master wafers at 70 °C as described previously.<sup>30,31</sup> A simple aspiration pumping system was used to introduce all solutions through the microchannels. A solution of the bifunctional linker SPDP (6.4 mM in 0.1 M PBS, pH 7.4) was introduced into the microchannels and allowed to react with the MUAM surface for 2 h. The NHS ester of SPDP reacts with the terminal amines of the monolayer to form a covalent amide linkage creating a disulfide-terminated surface. Solutions of cysteine-modified peptides (2 mM in 0.1 M PBS, pH 7.4) were introduced into each microchannel and immobilized overnight via a thiol–disulfide reaction. The inset in Figure 1 shows a schematic depiction of the immobilized peptide surface chemistry. The efficiency of each step of this highly reproducible peptide im-

- (12) Rodriguez, M.; Li, S.; Harper, J.; Zhou, S. *J. Biol. Chem.* **2004**, *279*, 8802–8807.
- (13) Fujii, T.; Kunimatsu, M. *Biol. Pharm. Bull.* **2003**, *26*, 771–774.
- (14) Mazor, Y.; Gilead, S.; Benhar, I.; Gazit, E.; Wise, G. S. *J. Mol. Biol.* **2002**, *322*, 1013–1024.
- (15) Reineke, U.; Ivascu, C.; Schlieff, M.; Landgraf, C.; Gericke, S.; Zahn, G.; Herzel, H.; Volkmer-Engert, R.; Schneider-Mergener, J. *J. Immunol. Methods* **2002**, *267*, 37–51.
- (16) Lesaichere, M. L.; Uttamchandani, M.; Chen, G.; Yao, S. Q. *Bioorg., Med. Chem. Lett.* **2002**, *12*, 2085–2088.
- (17) Hilper, K.; Hansen, G.; Wessner, H.; Schneider-Mergener, J.; Hohne, W. J. *Biochem.* **2000**, *128*, 1051–1057.
- (18) Houseman, B. T.; Huh, J. H.; Kron, S. J.; Mrksich, M. *Nat. Biotechnol.* **2002**, *20*, 270–274.
- (19) Dekker, N.; Cox, R. C.; Kramer, A.; Egmond, M. R. *Biochemistry* **2001**, *40*, 1694–1701.
- (20) Frank, R. *Comb. Chem. High Throughput Screening* **2002**, *5*, 429–440.
- (21) Kato, R.; Kunimatsu, M.; Fujimoto, S.; Kobayashi, T.; Honda, H. *Biochem. Biophys. Res. Commun.* **2004**, *315*, 22–29.
- (22) Dong, L.; Hulsmeyer, M.; Durkop, H.; Hansen, H. P.; Schneider-Mergener, J.; Ziegler, A.; Uchanska-Ziegler, B. *J. Mol. Recognit.* **2003**, *16*, 28–36.
- (23) Melnyk, O.; Duburcq, X.; Olivier, C.; Urbes, F.; Auriault, C.; Gras-Masse, H. *Bioconjugate Chem.* **2002**, *13*, 713–720.
- (24) Wegner, G. J.; Lee, H. J.; Corn, R. M. *Anal. Chem.* **2002**, *74*, 5161–5168.
- (25) Andersson, K.; Areskoug, D.; Hardenborg, E. *J. Mol. Recognit.* **1999**, *12*, 310–315.
- (26) Chinowsky, T. M.; Quinn, J. G.; Bartholomew, D. U.; Kaiser, R.; Elkind, J. L. *Sens. Actuators, B.* **2003**, *B91*, 266–274.
- (27) Suzuki, M.; Ozawa, F.; Sugimoto, W.; Aso, S. *Anal. Bioanal. Chem.* **2002**, *372*, 301–304.
- (28) Shumaker-Parry, J. S.; Campbell, C. T. *Anal. Chem.* **2004**, *76*, 907–917.
- (29) Shumaker-Parry, J. S.; Zareie, M. H.; Aebersold, R.; Campbell, C. T. *Anal. Chem.* **2004**, *76*, 918–929.

(30) Lee, H. J.; Goodrich, T. T.; Corn, R. M. *Anal. Chem.* **2001**, *73*, 5525–5531.

(31) Duffy, D. C.; McDonald, J. C.; Schueller, O. J. A.; Whitesides, G. M. *Anal. Chem.* **1998**, *70*, 4974–4984.

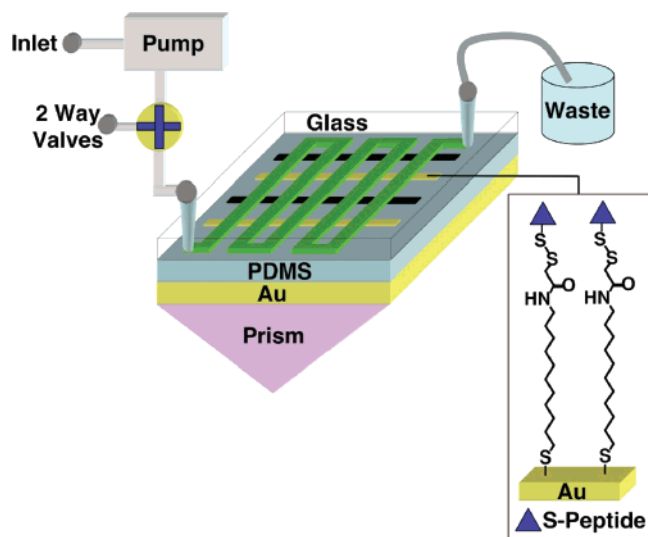


Figure 1. Schematic representation of sample apparatus used for SPR imaging kinetic measurements. A peptide line array is fabricated on a gold thin film and optically coupled to a glass prism. A serpentine microchannel is placed perpendicular to the line array and used as a flow cell to deliver buffer and analyte. The inset shows the surface chemistry used to covalently attach a cysteine-terminated peptide to a chemically modified self-assembled monolayer on a gold thin film.

mobilization process has been extensively characterized and is reported elsewhere.<sup>24</sup> The surface coverage of the peptide monolayer was determined to be  $1.5 (\pm 0.1) \times 10^{13}$  molecules/cm<sup>2</sup> by using fluorescence wash-off measurements of labeled peptides after cleavage of the surface disulfide bond.<sup>24</sup> To create NVOC-protected S peptide (NVOC-S1), the lysines and N-terminus of S1 peptide were reacted with NVOC-Cl.<sup>32</sup> The microchannels were then removed and the array was exposed to PEG-NHS (4 mM in 0.1 M TEA, pH 8.0) for 40 min to prevent nonspecific protein adsorption to the areas between the immobilized peptides. Further details of the array fabrication process are reported elsewhere.<sup>24,30</sup>

**Kinetic Flow Cell Design.** To achieve continuous sample delivery to the peptide array during kinetics experiments, a small-volume microfluidics system was designed. Figure 1 shows a schematic of the prism-sample apparatus used to perform real-time SPR imaging measurements. The flow cell was created by placing a microchannel (670- $\mu$ m width, 9.5-cm total length, 200- $\mu$ m depth) in contact with the sample surface. This microchannel wrapped around the sample surface with 400- $\mu$ m spacing between folds and had a total sample volume of 13  $\mu$ L. Discrete SPR imaging probe regions were formed by orienting the microchannel perpendicular to the peptide line array. Each of these peptide regions were 300  $\mu$ m by 670  $\mu$ m in size with a maximum number of 50 sample probe areas on a single chip surface. The microchannels were created by replication from a 3D aluminum master. This mold was filled with degassed PDMS, covered with a glass slide to create a flat surface, and cured at 70 °C. A key feature of this design is the edges of the channel walls are defined by a ridge machined deeper into the aluminum master than any other area of the mold. This ridge results in the formation of a tight "O-ring" seal when the PDMS layer is sandwiched between the chip surface and a glass backing plate equipped with inlet and outlet ports for solution delivery. The aluminum holder supporting

the sample assembly was also carefully designed to prevent overcompression of the PDMS flow cell, yet provide an adequate seal to avoid solution leakage. Immediately prior to cell assembly, the PDMS channel was placed in a plasma oxidation chamber for 30 s. This process improved the hydrophilicity of the PDMS surface<sup>33,34</sup> and significantly reduced nonspecific adsorption of protein. Solutions were delivered using a peristaltic pump with a maximum flow rate of 1 mL/min, and a valve was installed at the inlet port to switch between sample and buffer solutions. A dead time of 4.2 s was measured when sample and buffer solutions were exchanged. SPR imaging kinetics experiments were performed using a continuous flow of solution to prevent mass transport limitations, while the equilibrium measurements were obtained under stopped-flow conditions.

**Real-Time SPR Imaging Measurements.** An SPR imaging apparatus (GWC Technologies) using near-infrared excitation from a collimated incoherent white light source as previously described<sup>35</sup> was used for the real-time monitoring of protein adsorption/desorption and surface enzyme kinetics. Briefly, p-polarized light is directed toward a sample prism assembly (Figure 1) at a fixed angle. Light reflected from this assembly is passed through a narrow band-pass filter and focused through a collection lens onto a CCD camera. The video image is digitized using a framegrabber card (PIXCI, Epix, Inc.) at a capture rate of 30 frames/s with the image acquisition controlled using V++ software (Digital Optics). A key feature of this software is the ability to write custom macros, which allows the user to define any number of regions of interest (ROIs) on the array surface. Figure 2a shows an SPR image of a peptide array mounted perpendicular to the PDMS flow cell. The dotted lines indicate the boundaries of the ROIs on the chip including peptide array elements for protein binding and PEG-terminated regions, which serve as a protein-resistant background.

Kinetics data for each ROI were collected by measuring the change in percent reflectivity as a function of time. A reference image was taken prior to protein introduction, and the average pixel intensity for each ROI recorded. The change in average pixel intensity with respect to the corresponding reference value was then recorded for each ROI. A graphical display, updated in real time, allowed changes in the pixel intensity for different array elements to be monitored and compared over the course of an experiment. The time interval between measurements and the number of frames averaged before ROI analysis was adjusted depending on the experimental time scale. Typically, a five-frame averaged image would be saved and analyzed with a time resolution of  $\sim 1$  s. Figure 2b shows the change in signal for a selection of probe ROIs as a function of time while protein solution is introduced through the flow channel. The difference in percent reflectivity ( $\Delta\%R$ ) for each of the probe areas was normalized to the average of the  $\Delta\%R$  measured for the PEG background ROIs adjacent to each peptide element. This analysis corrected for changes in bulk refractive index and nonspecific protein adsorption. All data processing and kinetic model fitting were performed using the software packages Microsoft Excel and Igor Pro.

(32) Marriott, G. *Biochemistry* **1994**, *33*, 9092–9097.

(33) Chaudhury, M. K.; Whitesides, G. M. *Langmuir* **1991**, *7*, 1013–1025.

(34) Lee, J. N.; Park, C.; Whitesides, G. M. *Anal. Chem.* **2003**, *75*, 6544–6554.

(35) Nelson, B. P.; Frutos, A. G.; Brockman, J. M.; Corn, R. M. *Anal. Chem.* **1999**, *71*, 3928–3934.

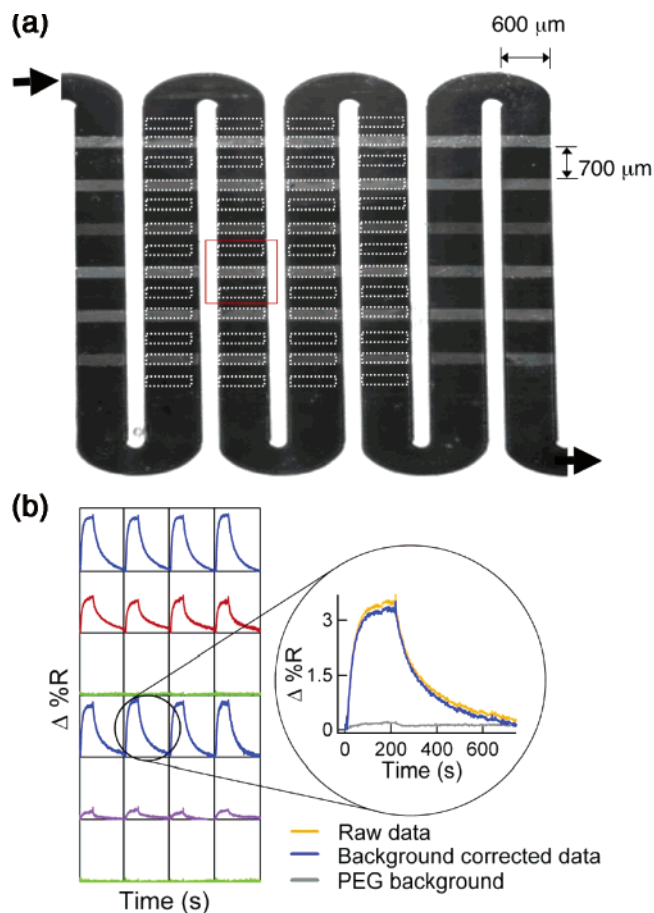


Figure 2. (a) Representative raw SPR image of a peptide array used as a mask for kinetics experiments. The dotted lines indicate ROIs on the array, where the change in percent reflectivity is measured as a function of time using a CCD camera. (b) Representative graphs showing the kinetics information obtained for each peptide element on the array, normalized with respect to adjacent PEG regions, while a 150 nM solution of S protein and buffer is sequentially introduced.

**Kinetics Methodology.** Surface-based kinetic measurements of protein–peptide binding interactions are a powerful tool for determining the rate constants of adsorption ( $k_a$ ) and desorption ( $k_d$ ). Figure 3 illustrates representative kinetics data obtained by monitoring the change in percent reflectivity caused by the adsorption and desorption of protein to immobilized peptide probes. This plot is the average of the change in percent reflectivity observed for five peptide regions normalized with respect to the PEG backgrounds, as described in the section above. Excellent reproducibility of the kinetics measurements was observed from chip to chip with variations in measured adsorption and desorption rate constants of  $\sim 5\%$ . When a continuous flow of protein solution is injected over the array, adsorption of protein on the peptide surface occurs. If the injection proceeds for a sufficiently long time, a steady state is reached where adsorption and desorption rates are equal. After the sample solution is replaced with buffer, the bound protein desorbs from the surface and the bare peptide array is regenerated.

To effectively analyze the kinetic data obtained for protein–peptide interactions, sequential fitting of the desorption and adsorption phases was employed to measure values of  $k_d$  and  $k_a$ . All protein–peptide adsorption and desorption measurements

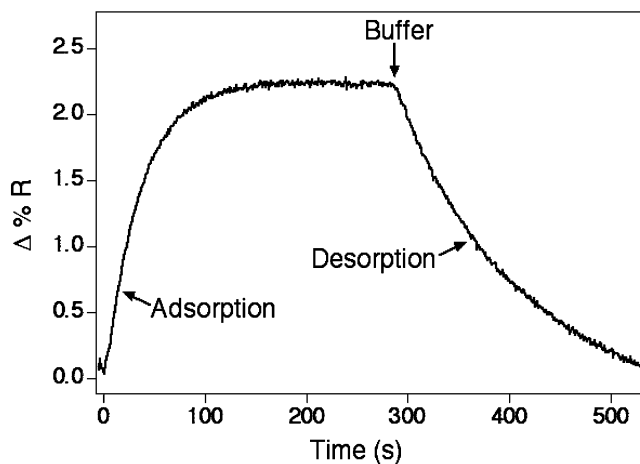


Figure 3. Change in percent reflectivity over time as protein solution and buffer were sequentially injected over a peptide array. Initially, adsorption of protein on the peptide surface is observed as a continuous flow of protein solution is introduced to the array. A steady state is reached where the rates of protein adsorption and desorption are equal. Desorption of the protein from the surface is observed when the constant flow of protein solution is replaced with buffer. This curve was obtained by averaging the change in percent reflectivity measured at five peptide array elements relative to the PEG background.

reported in this paper were analyzed based on a simple 1:1 interaction between a protein analyte and a surface-immobilized peptide probe (i.e.,  $A + B \leftrightarrow AB$ ). First, in terms of SPR response ( $\Delta\%R$ ), the rate of desorption of the complex AB can be described by

$$\Delta\%R(t) = \Delta R \exp(-k_d t) \quad (1)$$

where  $\Delta R$  corresponds to the maximum change in SPR signal measured at each protein concentration.<sup>36</sup> The desorption rate constant  $k_d$  is independent of protein concentration. An initial appreciation of the magnitude of  $k_d$  from the protein desorption measurements can be advantageous because in cases where  $k_d$  is sufficiently small, the adsorption curve contains little information about the desorption process.

Next, the adsorption curve was analyzed to obtain values for the association rate constant,  $k_a$ , as well as providing an independent determination of  $k_d$ . The net rate of protein–peptide complex formation can be described as

$$\Delta\%R(t) = \frac{k_a C \Delta R_{\max}}{k_a C + k_d} \{1 - e^{-(k_a C + k_d)t}\} \quad (2)$$

where  $C$  is the protein analyte solution concentration and  $\Delta R_{\max}$  refers to the maximum SPR signal obtained when all surface binding sites are occupied.<sup>36</sup> Equation 2 can be simplified using the Langmuir adsorption isotherm<sup>37</sup> to

$$\Delta\%R(t) = \Delta R_{\max} \theta (1 - e^{-\gamma t}) \quad (3)$$

where  $\theta$  is the fraction of the total surface coverage and

$$\gamma = k_a C + k_d \quad (4)$$

Equation 3 is used to fit the adsorption data and determine values for  $\gamma$  and the product of  $\Delta R_{\max}\theta$  for multiple protein concentrations. Values of  $k_a$  and  $k_d$  are determined from the slope and  $y$ -intercept, respectively, of the linear plot of  $\gamma$  versus concentration. As a final point, the equilibrium adsorption coefficient,  $K_{\text{Ads}}$ , which represents the binding affinity between probe and analyte, can be derived from the ratio of the measured rate constants ( $K_{\text{Ads}} = k_a/k_d$ ). An alternative method for evaluating  $K_{\text{Ads}}$  is to plot the fractional surface coverage ( $\theta$ ), which is related to the final steady-state level under constant protein flow, as a function of protein concentration. These data can then be fit using a Langmuir adsorption isotherm, assuming the peptide monolayer is uniform and protein adsorption to each immobilized peptide is independent of protein adsorption to neighboring peptides.<sup>37</sup>

## RESULTS AND DISCUSSION

**Kinetics of S Protein Adsorption and Desorption onto Peptide Arrays.** We chose to examine the S protein–S peptide interaction because of the importance of this binding pair in the purification of fusion proteins.<sup>38–40</sup> S protein and S peptide originate from fragments of RNase A<sup>41,42</sup> and are of special interest because the protein–peptide complex has enzymatic activity comparable to the intact enzyme. This interaction was an ideal candidate for studying the kinetics of adsorption and desorption because of the excellent reversibility of the S protein–S peptide complex binding, with very little S protein denaturation onto immobilized peptides. In this section, we characterize the adsorption and desorption kinetics for the following: (i) the interaction of S protein with N terminal-immobilized wild-type S peptide (S1) and (ii) S protein interactions with three S peptide variants including a peptide derived from phage display (LB2), C terminal-immobilized S peptide (S2), and an NVOC-protected S peptide (NVOC-S1). All kinetic values were determined based on the kinetics methodology described in the Experimental Section.

**A. Wild-Type S1 Peptide–S Protein Adsorption and Desorption Kinetics.** Desorption measurements of S protein from wild-type S1 peptide for a number of different protein concentrations are displayed in Figure 4. To facilitate a direct comparison of the desorption curves, each data set was normalized with respect to the maximum steady-state signal obtained for each concentration prior to desorption. Normalized desorption curves for all protein concentrations display the same relationship, demonstrating that the rate of desorption is independent of initial S protein surface coverage. The inset in Figure 4 shows a natural log plot of the normalized desorption curves as a function of time. By applying eq 1, a  $k_d$  of  $1.0 (\pm 0.08) \times 10^{-2} \text{ s}^{-1}$  for the S1–S protein interaction was measured from the slope of the linear fit for each curve.

A series of adsorption curves observed for S protein concentrations ranging from 10 to 300 nM to immobilized S1 peptide are

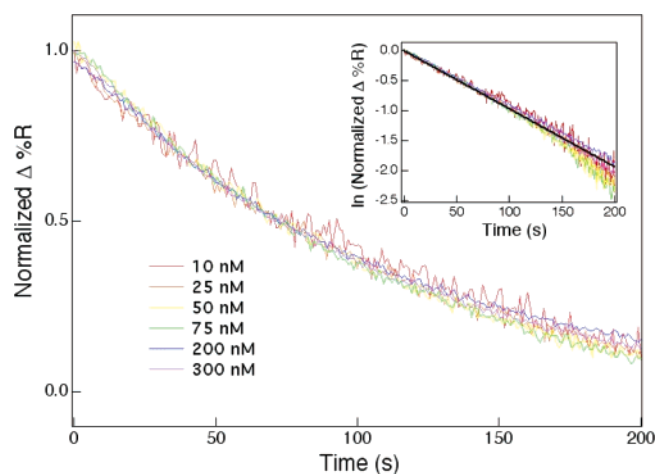


Figure 4. Change in percent reflectivity as a function of time as S protein desorbs from an S peptide-modified surface. Since desorption is not dependent on the initial surface coverage of S protein, all concentrations display the same dissociation curve when the data are normalized. Inset shows the natural log plot of the normalized signal for multiple concentrations versus time. The value of  $k_d$  was determined by the linear slope of these data to be  $1.0 (\pm 0.08) \times 10^{-2} \text{ s}^{-1}$ .

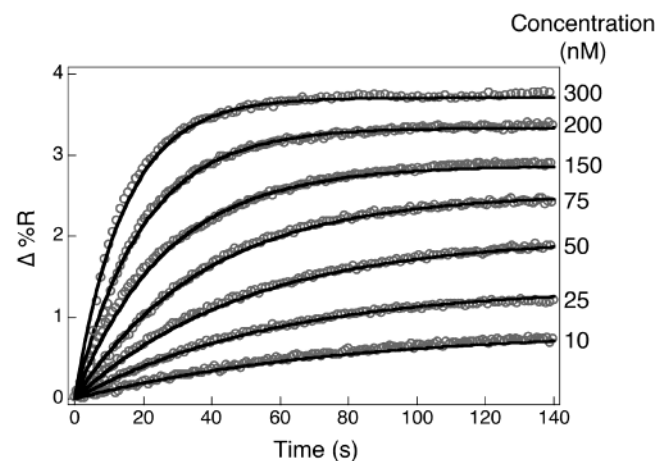


Figure 5. Compiled kinetics data for the adsorption of several concentrations of S protein onto an S peptide array. These data were fit using eq 3. Separate experiments were performed for each protein concentration, and each adsorption curve is an average of five individual array elements. The protein concentration ranged from 10 to 300 nM.

summarized in Figure 5. The adsorption rate constant was determined from these data using eqs 3 and 4. The  $\gamma$  values for each protein concentration, evaluated using eq 3, are plotted in Figure 6. This plot displays excellent linearity, and the slope was used to determine the value of  $k_a$  to be  $1.9 (\pm 0.05) \times 10^5 \text{ M}^{-1} \text{ s}^{-1}$ . The  $k_d$  value was measured from the  $y$ -intercept as  $1.1 (\pm 0.08) \times 10^{-2} \text{ s}^{-1}$ , which is in very close agreement with the value independently determined from the desorption curves above. An equilibrium adsorption constant ( $K_{\text{Ads}}$ ) of  $1.7 (\pm 0.1) \times 10^7 \text{ M}^{-1}$  was determined from the ratio of  $k_a$  and  $k_d$ .

The  $K_{\text{Ads}}$  determined from the rate constants was compared to the value determined from equilibrium adsorption isotherms. Figure 7 shows the change in percent reflectivity plotted as a function of S protein for two sets of data. The change in percent reflectivity for multiple S protein concentrations was compiled

- (36) O'Shannessy, D. J.; Brigham-Burke, M.; Soneson, K. K.; Hensley, P.; Brooks, I. *Anal. Biochem.* **1993**, *212*, 457–468.
- (37) Adamson, A. W.; Gast, A. P. *Physical Chemistry of Surfaces*, 6th ed.; John Wiley & Sons Inc.: New York, 1999.
- (38) Kim, J.; Raines, R. T. *Protein Sci.* **1993**, *2*, 348–356.
- (39) Senchenko, V. N.; Dianova, M. V.; Kanevsky, V. Y.; Bocharova, A. L.; Karpeisky, M. Y. *Mol. Biol.* **1993**, *27*, 565–569.
- (40) Kim, J.; Raines, R. T. *Anal. Biochem.* **1994**, *219*, 165–166.
- (41) Kim, E. E.; Varadarajan, R.; Wyckoff, H. W.; Richards, F. M. *Biochemistry* **1992**, *31*, 12304–12314.
- (42) Raines, R. T. *Chem. Rev.* **1998**, *98*, 1045–1065.

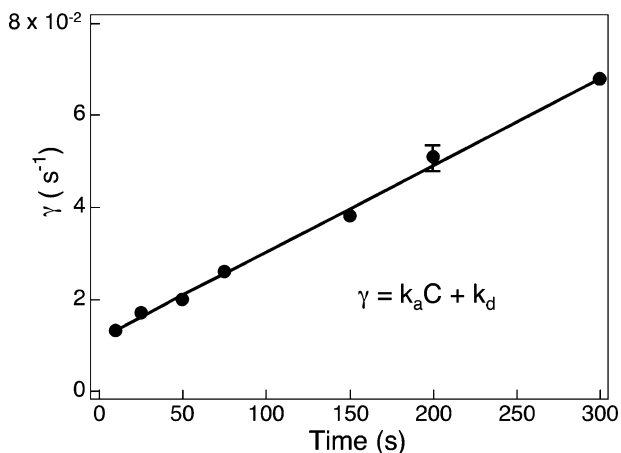


Figure 6. Plot of  $\gamma$  values, obtained from the S protein adsorption curves in Figure 5, as a function of S protein concentration. The linear slope corresponds to the adsorption rate constant,  $k_a$ , with a value of  $1.9 (\pm 0.05) \times 10^5 \text{ M}^{-1} \text{ s}^{-1}$ , and the y-intercept corresponds to the desorption rate constant,  $k_d$ , determined to be  $1.1 (\pm 0.08) \times 10^{-2} \text{ s}^{-1}$ .

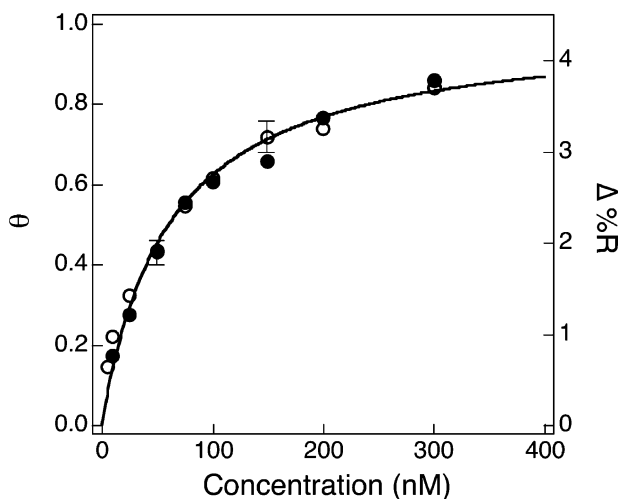


Figure 7. Langmuir isotherm fits of equilibrium and kinetic measurements of S protein adsorption onto S1 array elements. Equilibrium measurements were performed by introducing aliquots of increasing S protein concentrations over the array surface and measuring the  $\Delta\%R$  after 15 min, for each concentration. The maximum signal for the kinetics experiments were determined from the fit of the adsorption curve. The data for equilibrium ( $\circ$ ) and kinetic measurements ( $\bullet$ ) are plotted as a function of concentration, and the Langmuir isotherm fit for both is shown by a solid line. The adsorption constant  $K_{\text{Ads}}$  was determined to be  $1.7 (\pm 0.08) \times 10^7 \text{ M}^{-1}$  by both methods.

using stopped-flow SPR measurements ( $\circ$ ).  $\theta$  values were also analyzed using eq 3, described in the Experimental Section, when fitting the S1 peptide–S protein adsorption curves in Figure 4 ( $\bullet$ ). These data sets were fit with Langmuir adsorption isotherms, and the  $K_{\text{Ads}}$  for both was determined to be  $1.7 (\pm 0.08) \times 10^7 \text{ M}^{-1}$ . The  $K_{\text{Ads}}$  for the interaction of S protein with immobilized wild-type S peptide is well within the reported range of binding constants from  $1.7 \times 10^6$  to  $1.5 \times 10^8 \text{ M}^{-1}$ .<sup>43–47</sup> The considerable

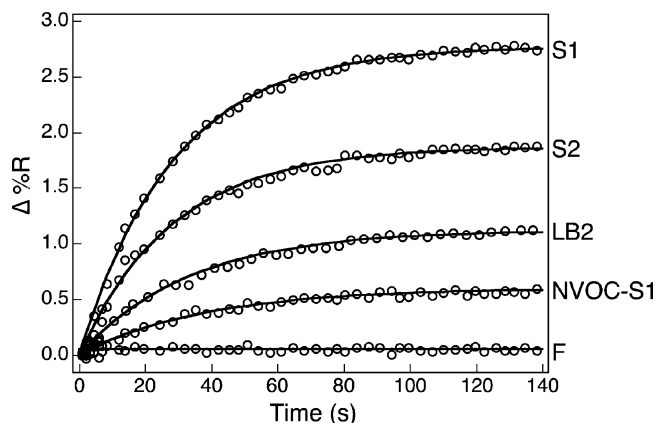


Figure 8. Kinetics data obtained from the adsorption of 150 nM S protein onto a peptide array composed of N and C terminal-immobilized wild-type S peptide (S1 and S2), a mutant S peptide (LB2), an NVOC-protected S peptide (NVOC-S1), and FLAG peptide (F). The adsorption curves were fitted using eq 3. Differential binding to the immobilized peptide probes is observed.

Table 2. Constants for S Peptide Derivative Derived by Adsorption Kinetics

peptide	$k_a (\text{M}^{-1} \text{s}^{-1})$	$k_d (\text{s}^{-1})$	$K_{\text{Ads}} (\text{M}^{-1})$
S1	$1.9 (\pm 0.05) \times 10^5$	$1.1 (\pm 0.08) \times 10^{-2}$	$1.7 (\pm 0.08) \times 10^7$
S2	$1.6 (\pm 0.04) \times 10^5$	$1.1 (\pm 0.07) \times 10^{-2}$	$1.5 (\pm 0.07) \times 10^7$
LB2	$1.2 (\pm 0.05) \times 10^5$	$1.1 (\pm 0.03) \times 10^{-2}$	$1.1 (\pm 0.05) \times 10^7$
NVOC-S1			$\sim 1.0 \times 10^7$
F			

variations in the reported S peptide–S protein binding constant reflect the diversity of the systems examined including gels,<sup>46</sup> solution-based measurements,<sup>44,45,47</sup> and adsorption of solution-phase peptides onto S protein immobilized in a dextran layer.<sup>43</sup>

**B. Multiplexed Determination of S Protein Adsorption/Desorption Kinetics.** To demonstrate the utility of SPR imaging to adsorption/desorption kinetics in an array format, S protein interactions with four S peptide derivatives were studied in a single experiment. These multiplexed kinetics experiments were performed to investigate the effects of peptide orientation and sequence variation on S protein adsorption. Figure 8 depicts the adsorption of 150 nM S protein onto a multicomponent peptide array. The kinetics data obtained from the adsorption interactions of S protein at multiple concentrations is summarized in Table 2. These data indicate that variations of peptide sequence and orientation have a more significant effect on  $k_a$  than  $k_d$ . Similar equilibrium adsorption constants were measured for S1 and LB2, with slightly weaker affinities observed for LB2 (35% smaller) than the wild-type peptide S1. The affinity of S protein to LB2 has been reported to be stronger (100 times) than the wild-type S peptide by an alternate experimental approach employing immobilized S protein in a dextran layer.<sup>43</sup> A C terminal-immobilized S peptide (S2) was used to evaluate the effect of peptide orientation on S protein adsorption, with a slightly higher affinity (20%) observed for the N terminal-immobilized S1 peptide compared to S2. The difference in steady-state SPR signal may be attributed to the

(43) Dwyer, J. J.; Swyer, M. A.; Kossiakoff, A. A. *Biochemistry* **2001**, *40*, 13941–13500.

(44) Connelly, P. R.; Varadarajan, R.; Sturtevant, J. M.; Richards, F. M. *Biochemistry* **1990**, *29*, 6108–6114.

(45) Hearn, R. P.; Richards, F. M.; Sturtevant, J. M.; Watt, G. D. *Biochemistry* **1971**, *10*, 806–817.

(46) Park, S.; Raines, R. T. *Protein Sci.* **1997**, *6*, 2344–2349.

(47) Goldberg, J. M.; Baldwin, R. L. *Proc. Natl. Acad. Sci. U.S.A.* **1999**, *96*, 2019–2024.

presence of cysteine-containing peptide fragments present in the S2 sample but not in the S1 sample. This resulted in a greater surface coverage of full-length S1 peptides compared to S2 peptides. Last, less S protein adsorption was observed to the NVOC-S1 peptide compared to the original S1 peptide. These data show it is possible to moderate protein adsorption to immobilized S1 peptide by blocking the lysine residues and the N terminus of this peptide with the bulky, photolabile NVOC protecting group. Adsorption and desorption rate constants were not determined for NVOC-S1 because the SPR signal was too low to accurately perform a full analysis of  $k_a$  and  $k_d$  at multiple S protein concentrations below 150 nM. Instead, the  $K_{Ads}$  for NVOC-S1 was estimated by using a Langmuir isotherm to fit the concentration dependence of the steady-state SPR signal and was found to be about the same value as that determined for the S1-S protein. This  $K_{Ads}$  value and the steady-state SPR signal observed for NVOC-S1 suggest that the NVOC groups block S protein adsorption to 80% of the immobilized S1 peptides, while the remaining 20% of S1 peptides are not modified with NVOC and are fully functional.

**Sequence-Specific Enzymatic Reactions of Factor Xa and Peptide Arrays.** The enzymatic reactions of factor Xa were examined as a second example of real-time SPR imaging measurements of peptide arrays. In vivo, factor Xa cleaves the protein prothrombin to create thrombin. Thrombin then activates fibrinogen, resulting in fibrin formation and the induction of blood clotting.<sup>48,49</sup> Factor Xa was selected for study because of its crucial role in the coagulation cascade and its utility in clinical assays for hemophilia based on factor X deficiency. Factor Xa activity was studied using a three component peptide array composed of substrate (P1), mutant substrate (P2), and a FLAG peptide control (F). The substrate peptide contained the known factor Xa recognition sequence from prothrombin<sup>50,51</sup> appended to the FLAG peptide sequence. Since factor Xa primarily cleaves after the arginine residue of the recognition motif, a decrease in percent reflectivity is observed as the FLAG sequence is removed from the surface by factor Xa (see Figure 9a). The mutant peptide contained the same sequence as the substrate peptide except the arginine residue was replaced with alanine. Peptide sequences are listed in Table 1.

Figure 9b shows the results of the enzymatic cleavage reaction performed by introducing a 1  $\mu$ M solution of factor Xa to this peptide array. These data were obtained by averaging the signal of five peptide elements normalized with respect to the PEG background. A significant decrease in signal was observed as factor Xa cleaves the FLAG portion of P1 from the surface. In contrast, much less P2 cleavage was observed, showing proteolytic cleavage by factor Xa is substantially reduced by the single amino acid change. There was little change in signal over time for the FLAG control peptide, suggesting that factor Xa does not non-specifically interact with this sequence. The P1 reaction curve shows a first-order exponential decrease in immobilized peptide substrate with time. The rate of the enzymatic cleavage reactions

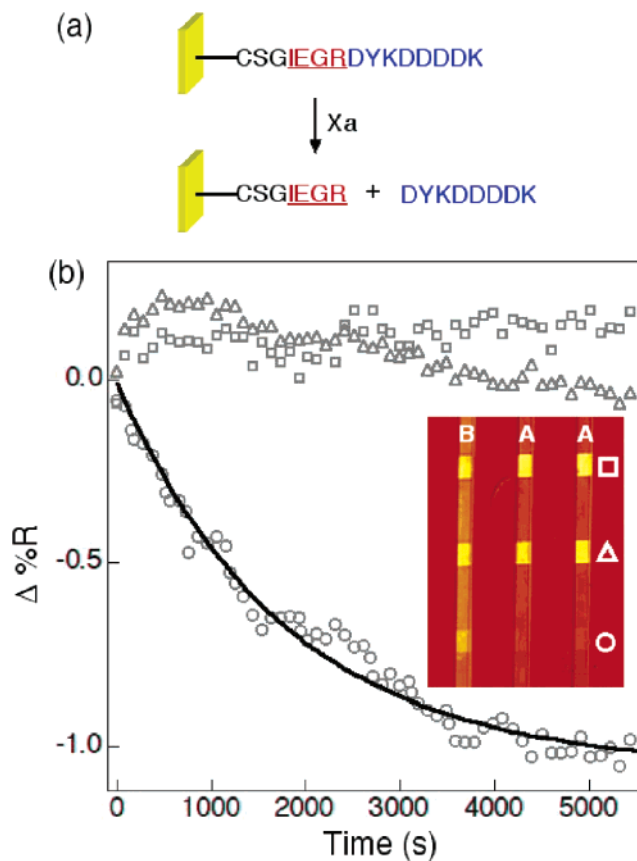


Figure 9. (a) Schematic showing the reaction of factor Xa with immobilized peptides. The substrate is composed of the cleavage site for factor Xa and an extension containing the FLAG sequence. When factor Xa cleaves the peptide, the FLAG portion is removed from the surface. (b) Plot showing the reaction of factor Xa with peptide substrate (P1,  $\circ$ ), mutant substrate (P2,  $\Delta$ ), and FLAG peptide control (F,  $\square$ ). P1 is cleaved from the surface at a much faster rate than P2, while no cleavage of F is observed. Inset shows an SPR difference image after 50 nM anti-FLAG solution is introduced to a peptide line array composed of F, P1, and P2. A set of parallel microchannels (labeled A and B) is placed perpendicular to the peptide line array. In both A channels, factor Xa is injected and reacted with the immobilized peptides for 2 h, while the B channel contained buffer. Anti-FLAG adsorption is observed for all peptides in the buffer channel. Insignificant anti-FLAG adsorption is observed for the substrate peptide (P1) after factor Xa reaction, indicating the FLAG portion of this sequence has been removed.

was determined from the slopes of the natural log of the data presented in Figure 9b. The velocities for the reactions of factor Xa with P1 and P2 were measured to be  $5.6 (\pm 0.3) \times 10^{-4}$  and  $5.7 (\pm 0.3) \times 10^{-5} \text{ s}^{-1}$ . These reaction rates indicate that the substrate (P1) is cleaved  $\sim 10$  times faster than the mutant peptide (P2).

In addition to enzyme kinetics, the interaction of anti-FLAG with the FLAG component of the P1, P2, and F peptides was used to ascertain the extent of proteolytic cleavage by factor Xa on a peptide array. The inset in Figure 9b presents a SPR difference image of the sequence-specific adsorption of anti-FLAG onto elements on the peptide array reacted with factor Xa or exposed to a buffer control. These experiments were performed using a parallel set of microchannels placed perpendicular to the peptide line array. Two microchannels (A) were exposed to a solution of 1  $\mu$ M factor Xa, while one microchannel (B) was exposed to buffer.

(48) Mann, K. G.; Butenas, S.; Brummel, K. *Arterioscler., Thromb., Vasc. Biol.* **2003**, *23*, 17–25.

(49) Rai, R.; Sprengeler, P. A.; Elrod, K. C.; Young, W. B. *Curr. Med. Chem.* **2001**, *8*, 101–119.

(50) Bianchini, E. P.; Louvain, V. B.; Marque, P. E.; Juliano, M. A.; Juliano, L.; Le Bonniec, B. F. *J. Biol. Chem.* **2002**, *277*, 20527–20534.

(51) Bang, N. U.; Mattler, L. E. *Haemostasis* **1978**, *7*, 98–104.

After reaction for 2 h, all three channels were rinsed vigorously with buffer. A 50 nM solution of anti-FLAG was then injected through all three channels. The difference image was obtained by subtracting images taken directly before and after the introduction of anti-Flag to the array surface. In channel B, where only buffer is introduced, anti-FLAG adsorption to all three peptide components P1, P2, and F is observed. Conversely, the A channels exposed to factor Xa show little antibody adsorption to the P1 elements due to the cleavage of the FLAG motif from the surface. More quantitatively, analysis of line profiles across channels A and B showed that ~90% of the FLAG sequence from the P1 elements was removed from the surface, while little P2 and F cleavage was observed. These results confirm the sequence selectivity of factor Xa observed using real-time SPR imaging measurements.

#### CONCLUSIONS

In this paper, we studied two systems of protein–peptide interactions in array formats using real-time SPR imaging. SPR imaging measurements were successfully applied to the simultaneous determination of  $k_a$ ,  $k_d$ , and  $K_{Ads}$  values for S protein adsorption to multiple S peptide derivatives using a single chip. The effect of a single amino acid substitution on the rate of peptide cleavage by the protease factor Xa was also examined. Future work will focus on examining the RNase activity of the S protein–S

peptide complex on the surface. Kinetics analysis of this surface enzymatic activity as well as functional assays of factor Xa and other peptide-modifying enzymes are currently in progress. The peptide–protein kinetic measurements studied in this paper demonstrate the potential of real-time SPR imaging as a tool for proteomics studies. In addition to peptide–protein interactions, real-time SPR imaging will be extremely useful in the study of the sequence-specific DNA–protein interactions involved in transcription factor recognition.

#### ACKNOWLEDGMENT

This research is funded by the National Institute of Health (2ROI GM059622-04 and 1RO1 EB00269-02), the National Science Foundation (CHE-0133151), the University-Industry Research grant award (Acct 118-0406) provided by the University of Wisconsin, and in part by the Defense Advanced Research Projects Agency (F30602-91-2-05555). The authors also thank Hitachi Corp. for the support of T.S. at the University of Wisconsin. The authors also thank Prof. Gerard Marriott for his assistance with the reactions of NVOC-Cl and peptides.

Received for review April 15, 2004. Accepted July 8, 2004.

AC0494275